Random telegraph dispersion management: modulational instability

Andrea Armaroli, Matteo Conforti

Random telegraph dispersion-management: modulational instability

ANDREA ARMAROLI[1,2,*] AND MATTEO CONFORTI[1]

[1] *Univ. Lille, CNRS, UMR 8523-PhLAM-Physique des Lasers Atomes et Molécules, F-59000 Lille, France*
[2] *Università di Ferrara, Department of Engineering, via Saragat 1, I-44122, Ferrara, Italy*
[*] *andrea.armaroli@unife.it*

Abstract: We study modulational instability in a fiber system resembling a dispersion-managed link where the sign of the group-velocity dispersion varies randomly according to a telegraph process. We find that the instability gain of stochastic origin converges, for long fiber segment mean length (the inverse of the transition rate between the two values), to the conventional values found in a homogeneous anomalous dispersion fiber. For short fiber segments, the gain bands are broadened and the maximum gain decreases. By employing correlation splitting formulas, we obtain closed form equations that allow us to estimate the instability gain from the linearized nonlinear Schrödinger equation. We compare the analytical to the numerical results obtained in a Monte Carlo spirit. The analysis is proven to be correct not only for a fluctuating group-velocity dispersion, but also including fourth-order dispersion (both constant or varying according to a synchronous or independent telegraph process). These results may allow researchers to tailor and control modulational instability sidebands, with applications in telecommunications and parametric photon sources.

1. Introduction

Modulational instability (MI), *i.e.*, the destabilization of a uniform wavepacket by exponentially growing harmonic perturbations around its carrier frequency, is an ubiquitous phenomenon in nonlinear dispersive wave physics [1]. The first studies emerged in electromagnetic waves [2] and hydrodynamics [3, 4], and about two decades later the phenomenon was observed in optical fibers [5]. The basic ingredients that yield MI in a one dimensional homogeneous system are focusing cubic nonlinearity (like the Kerr effect in silica) and anomalous (negative) group-velocity dispersion (GVD).

Nevertheless, MI exists also in normal GVD, provided that high-order dispersion [6] or birefringence [7] are considered. Moreover, MI is observed in single-mode fibers in the normal GVD region also if the GVD is varied along the propagation direction. If the variation is periodic, the MI is equivalent to the destabilization of a harmonic oscillator subject to parametric forcing and is denoted as parametric MI [8–12]. A resonance is found for every integer order to correspond to a MI sideband: only a few of them are observable and their frequency separation from the carrier scales as the square root of their order.

Random variations of GVD were also the subject of extensive study. In the late 90s, the white noise process (an exactly solvable model) was considered [9, 13–15]. Only recently different random processes were considered: localized GVD kicks [16] or coloured processes of low-pass or band-pass type [17].

Up to this point, we mentioned only examples of (possibly large) GVD variations around a nonzero average GVD. Actually, to prevent the competition with conventional MI, which usually exhibits larger gain, normal average GVD is considered.

Conversely, systems with zero- or nearly zero-average GVD have attracted the attention of many researchers, because dispersion-induced pulse-broadening is largely suppressed and nonlinear propagation optimized [18, 19]. This strategy is usually denoted dispersion management (DM) and consists in alternating positive and negative GVD segments along the propagation direction. A uniform distribution for fluctuation of segment length is studied in [20, 21] for pulse propagation

and MI, respectively.

Here we adapt part of the theory presented in Ref. [17] to DM-like random fluctuations modelled as a telegraph process, *i.e.*, a low-pass colored random process taking only two values alternating at exponentially distributed distances. Thanks to correlation splitting formulas [22–27], the MI equations (i.e. the linearized uni-directional propagation equation) are also solvable.

Our theoretical approach is quite general and flexible, and permits to account for additional physical effects. As a relevant example, we explore the influence of the first higher-order effect having an impact on MI, *i.e.*, the fourth-order dispersion (FOD).

The rest of the paper is organized as follows. After presenting the model equations and detailing the analytical approach for fluctuations of GVD and (possibly) FOD in Sec. 2, we compare the analytical estimates to numerical results obtained in a Monte Carlo spirit in Sec. 3. Several different examples are discussed, including no FOD, fixed or fluctuating FOD. Conclusions are reported in Sec. 4.

2. Analytical approach

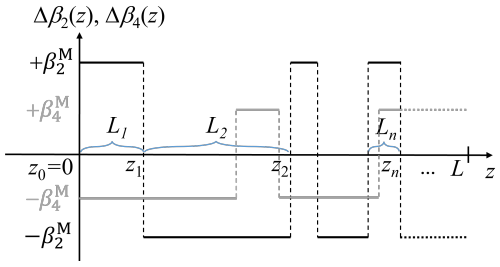

Fig. 1. Schematic representation of the GVD and FOD profiles in a typical fiber realization. The random distances of sign changes are shown only for GVD.

We consider the propagation of optical pulses ruled by the generalized nonlinear Schrödinger equation (GNLSE) [18],

$$i\partial_z U - \frac{1}{2}\beta_2(z)\partial_t^2 U + \frac{1}{24}\beta_4(z)\partial_t^2 U + \gamma|U|^2 U = 0, \tag{1}$$

where $U(t, z)$ is the complex envelope of the optical field, (t,z) are time and propagation distance in a frame moving at the group velocity of the fiber mode, γ the (constant) nonlinear coefficient, $\beta_2(z) = \bar{\beta}_2 + \Delta\beta_2(z)$ is the GVD, and $\beta_4(z) = \bar{\beta}_4 + \Delta\beta_4(z)$ is the FOD. Moreover, $\Delta\beta_2$ and $\Delta\beta_4$ are two telegraph processes. They can take only two values, $\pm\beta_2^{\mathrm{M}}$, with $\beta_2^{\mathrm{M}} > 0$, (resp. $\pm\beta_4^{\mathrm{M}}$, with $\beta_4^{\mathrm{M}} \geq 0$). We consider either (i) synchronous or (ii) independent (asynchronous) processes. The latter case is schematically illustrated in Fig. 1.

The samples of the dispersion profiles (GVD and FOD) are generated using the following procedure [28]. The total length L is fixed, then we extract for the i-th sample a positive integer N_i from a Poisson distribution with rate $L/\bar{L}_m$, $m = 2, 4$. We extract N_i points w_n, $n = 1, 2, \ldots, N_i$ from a uniform distribution in $[0, L]$, and order them in ascending order, to obtain the points z_i where the sign changes occurs (in the case of asynchronous GVD and FOD two independent sets of points are used). The lengths $L_n = z_n - z_{n-1}$ are independent, identically distributed random variables of exponential probability distribution function with mean $\bar{L}_m$, $m = 2, 4$, thus representing a telegraph process. The telegraph process is an example of lowpass colored noise, as discussed in detail in [17]. The bandwidth is inversely proportional to the mean length, $B_m = \frac{2}{\bar{L}_m}$.

A continuous wave (t-independent) solution of Eq. (1) reads $U_0(z) = \sqrt{P}\exp(i\gamma P z)$, where P is the carrier power. In order to study its stability, we insert in Eq. (1) the *Ansatz* $U(z,t) = \left[\sqrt{P} + \check{x}_1(z,t) + i\check{x}_2(z,t)\right]\exp(i\gamma P z)$, where $\check{x}_{1,2}$ are assumed to be small, linearize and Fourier-transform the resulting equation with respect to t (ω is used as the associated angular frequency detuning from the carrier U_0). We obtain

$$\frac{\mathrm{d}x}{\mathrm{d}z} = \begin{bmatrix} 0 & -g(z) \\ h(z) & 0 \end{bmatrix} x, \tag{2}$$

with $x \equiv (x_1, x_2)^{\mathrm{T}}$—$x_{1,2}$ are the Fourier transforms of $\check{x}_{1,2}$, functions of ω and z, $g(z) = \beta_2(z)\frac{\omega^2}{2} + \beta_4(z)\frac{\omega^4}{24} = g_0 + \delta g(z)$ and $h(z) = g(z) + 2\gamma P = h_0 + \delta g(z)$, with $g_0 \equiv \bar{\beta}_2\frac{\omega^2}{2} + \bar{\beta}_4\frac{\omega^4}{24}$, $h_0 \equiv g_0 + 2\gamma P$, $\delta g \equiv \Delta\beta_2(z)\frac{\omega^2}{2} + \Delta\beta_4(z)\frac{\omega^4}{24}$. Eq. (2) is a system of stochastic differential equations (SDEs) for each value ω.

By letting $\beta_2^{\mathrm{M}} = \beta_4^{\mathrm{M}} = 0$, Eq. (2) is reduced to a system of linear autonomous ordinary differential equations (ODEs) [6, 29]. Provided that $\bar{\beta}_2$ and $\bar{\beta}_4$ are not both positive, there exist intervals in ω for which the eigenvalues of the matrix in Eq. (2) are real and the MI gain thus reads

$$G(\omega) = \max\left[\mathrm{Re}\left\{\sqrt{-\left(\bar{\beta}_2\frac{\omega^2}{2} + \bar{\beta}_4\frac{\omega^4}{24}\right)\left(\bar{\beta}_2\frac{\omega^2}{2} + \bar{\beta}_4\frac{\omega^4}{24} + 2\gamma P\right)}\right\}\right]. \tag{3}$$

It is easy to verify (directly or by nonlinear phase-matching arguments) that this expression has maxima in

$$\omega^2 = -\frac{6\bar{\beta}_2}{\bar{\beta}_4}\left(1 \pm \sqrt{1 - \frac{2\gamma P}{3}\frac{\bar{\beta}_4}{\bar{\beta}_2^2}}\right), \tag{4}$$

(provided that $\omega^2 > 0$) at which, remarkably, G achieves the same value, $G_{\max} = \gamma P$, obtained in conventional MI. There exist three possible combinations of signs of $\bar{\beta}_2$ and $\bar{\beta}_4$ which lead to MI gain. For anomalous GVD and $\bar{\beta}_4 < 0$ a single sidelobe appears, which is a deformation of the conventional MI gain. If, instead, $\bar{\beta}_4 > 0$ and $\gamma P\frac{\bar{\beta}_4}{\bar{\beta}_2^2} \ll 1$, two MI sidelobes appear: the first is a slight variation of the conventional MI sidelobe in the absence of FOD, *i.e.*, $0 \le \omega \le 2\sqrt{\frac{\gamma P}{\bar{\beta}_2}}$ and the second occurs at $\omega \approx \sqrt{12\left|\frac{\bar{\beta}_2}{\bar{\beta}_4}\right|}$. Around this same value a single MI sidelobe appears for normal GVD and $\bar{\beta}_4 < 0$. For the sake of precision, we notice that the high frequency narrow MI sidebands are slightly different in anomalous vs. normal GVD for the same $|\bar{\beta}_4|$, as it is apparent from Eq. (4). Equations (3) and (4) will be important as limits of the analytical estimates presented below.

In the following we assume vanishing average GVD $\bar{\beta}_2 = 0$ (unless we refer to conventional MI, where $\bar{\beta}_2 = -1$); the average FOD $\bar{\beta}_4$ can take any positive or negative value.

In [30] a precise discussion of multiplicative noise (the fluctuation of the natural frequency of a harmonic oscillator, assumed non null) is presented. Its application to Eq. (2) was discussed in [17]: the unperturbed system is stable and the first moments $\langle x\rangle$ cannot provide any hint on the stability of the perturbed system. The equations for the second moments of the distribution of x, which are directly related to the fiber output power, need studying.

We let $X_1 = x_1^2$, $X_2 = x_2^2$, and $X_3 = x_1x_2$ and derive from Eq. (2)

$$\frac{\mathrm{d}}{\mathrm{d}z}X = \begin{bmatrix} 0 & 0 & -2g(z) \\ 0 & 0 & 2h(z) \\ h(z) & -g(z) & 0 \end{bmatrix} X, \tag{5}$$

with $X \equiv (X_1, X_2, X_3)^{\mathrm{T}}$. The following discussion relies only on Eq. (5). We first study the effect of fluctuations of GVD (with fixed average FOD), next we study the fluctuations of both GVD and FOD.

2.1. Fluctuations of GVD, $\beta_4^{\mathrm{M}} = 0$

Let us consider a constant FOD ($\Delta\beta_4 = 0$), therefore $\delta g = \Delta\beta_2(z)\frac{\omega^2}{2}$. The telegraph process allows for a particularly simple closure of the moment equations [25,26]. We apply to Eq. (5) the Shapiro-Loginov formula [24]

$$\langle \Delta\beta_2 \frac{\mathrm{d}X_i}{\mathrm{d}z} \rangle = \left(\frac{\mathrm{d}}{\mathrm{d}z} + B_2 \right) \langle \Delta\beta_2 X_i \rangle. \tag{6}$$

Two steps are required: (i) directly average Eq. (5), (ii) multiply each row by $\Delta\beta_2$ and average. Three auxiliary variables are introduced $X_{3+i} \equiv \Delta\beta_2 X_i$, for $i = 1, 2, 3$. Taking into account the property of telegraph processes, $\langle \Delta\beta_2^2 X_i \rangle = \sigma_2^2 \langle X_i \rangle$, with $\sigma_2^2 \equiv (\beta_2^{\mathrm{M}})^2$, we obtain a sixth order system of ODEs,

$$\frac{\mathrm{d}\langle X \rangle}{\mathrm{d}z} = \left[\begin{array}{c|c} A_4 & C_2 \\ \hline \sigma_2^2 C_2 & A_4 - B_2 \mathbf{I} \end{array} \right] \langle X \rangle, \tag{7}$$

with

$$\begin{aligned} A_4 &= \begin{bmatrix} 0 & 0 & -2g_0^{(4)} \\ 0 & 0 & 2h_0^{(4)} \\ h_0^{(4)} & -g_0^{(4)} & 0 \end{bmatrix}, \\ C_2 &= \begin{bmatrix} 0 & 0 & -\omega^2 \\ 0 & 0 & \omega^2 \\ \frac{\omega^2}{2} & -\frac{\omega^2}{2} & 0 \end{bmatrix}, \end{aligned} \tag{8}$$

with $g_0^{(4)} \equiv \bar{\beta}_4 \frac{\omega^4}{24}$, $h_0^{(4)} = g_0^{(4)} + 2\gamma P$ and $\mathbf{I}$ is the identify matrix. Eq. (7) is, *mutatis mutandis*, identical to Eq. (21) in [17].

The gain for the second moments is $G_2(\omega) \equiv \mathrm{Re}\,\tilde{\lambda}/2$, with $\tilde{\lambda}$ the eigenvalue of largest real part of the 6×6 matrix in Eq. (7). Recall that, for deterministic GVD [14], the gain associated to every moment is identical, thus G in Eq. (3) can be considered equivalent to G_2. By symbolic manipulations, it is easy to verify that, in the limit of $B_2 \to 0$, we obtain again the conventional MI gain, *i.e.*, Eq. (3) with $\pm\beta_2^{\mathrm{M}}$ in lieu of $\bar{\beta}_2$.

2.2. Synchronous fluctuations of GVD and FOD

Let us now consider a zero average FOD, but non-zero oscillations ($\bar{\beta}_4 = 0$, $\beta_m^M \neq 0$ for both $m = 2, 4$). First, we consider synchronous fluctuations, *i.e.*, a single process defined by a sample $\{z_n\}$ and $\beta_4^{\mathrm{M}} = \rho\beta_2^{\mathrm{M}}$, therefore $\delta g = \Delta\beta_2(z)(\frac{\omega^2}{2} + \rho\frac{\omega^4}{24})$. Following the same procedure and same variable definition of Sec. 2.1, we obtain

$$\frac{\mathrm{d}\langle X \rangle}{\mathrm{d}z} = \left[\begin{array}{c|c} A_0 & C_{24} \\ \hline \sigma_2^2 C_{24} & A_0 - B_2 \mathbf{I} \end{array} \right] \langle X \rangle, \tag{9}$$

with

$$A_0 = \begin{bmatrix} 0 & 0 & 0 \\ 0 & 0 & 4\gamma P \\ 2\gamma P & 0 & 0 \end{bmatrix},$$
$$C_{24} = \begin{bmatrix} 0 & 0 & -\omega^2 - \rho\frac{\omega^4}{12} \\ 0 & 0 & \omega^2 + \rho\frac{\omega^4}{12} \\ \frac{\omega^2}{2} + \rho\frac{\omega^4}{12} & -\frac{\omega^2}{2} - \rho\frac{\omega^4}{12} & 0 \end{bmatrix}, \tag{10}$$

Consider the limit $B_2, B_4 \to 0$: by symbolic manipulation, it is easy to verify that we obtain again Eq. (3) with $\pm\beta_m^{\mathrm{M}}$ in lieu of $\bar{\beta}_m$, for $m = 2, 4$, respectively. Thus, for $\rho > 0$ we obtain a single MI sideband, while for $\rho < 0$ we obtain also secondary sidelobes.

In contrast with the analysis of Eq. (7), there are different sign combinations that give MI gain, so we expect a combination of different MI sidelobes corresponding to different nonlinear phase-matching conditions to appear in G_2, at least in the limit of $\bar{L}_2, \bar{L}_4 \to \infty$.

2.3. Independent fluctuations of GVD and FOD

Let us consider again a zero average FOD, but non-zero independent oscillations ($\bar{\beta}_4 = 0$, $\beta_m^M \neq 0$ for $m = 2, 4$, $\langle \Delta\beta_2 \Delta\beta_4 \rangle = 0$ for all z).

The Shapiro-Loginov formula must be generalized, as in [17, 27, 31], to two independent random processes, as follows

$$\langle \Delta\beta_2 \Delta\beta_4 \frac{\mathrm{d}X_i}{\mathrm{d}z} \rangle = \left(\frac{\mathrm{d}}{\mathrm{d}z} + B_2 + B_4 \right) \langle \Delta\beta_2 \Delta\beta_4 X_i \rangle. \tag{11}$$

The derivation of a closed system of ODEs consists of four steps: (i) average directly Eq. (5), (ii) multiply each row of Eq. (5) by $\Delta\beta_2$ and average, (iii) multiply by $\Delta\beta_4$ and average; (iv) multiply by $\Delta\beta_2 \Delta\beta_4$ and average. If we assume as above that we can factor the variance out if the same process occurs twice inside an angle bracket, take statistical independence into account, and define $X_{3+i} \equiv \Delta\beta_2 X_i$, $X_{6+i} \equiv \Delta\beta_4 X_i$, and $X_{9+i} \equiv \Delta\beta_2 \Delta\beta_4 X_i$, $i = 1, 2, 3$ we obtain

$$\frac{\mathrm{d}\langle X \rangle}{\mathrm{d}z} = \left[\begin{array}{c|c|c|c} A_0 & C_2 & C_4 & \mathbf{0} \\ \hline \sigma_2^2 C_2 & A_0 - B_2\mathbf{I} & \mathbf{0} & C_4 \\ \hline \sigma_4^2 C_4 & \mathbf{0} & A_0 - B_4\mathbf{I} & C_2 \\ \hline \mathbf{0} & \sigma_4^2 C_4 & \sigma_2^2 C_2 & A_0 - (B_2 + B_4)\mathbf{I} \end{array}\right] \langle X \rangle, \tag{12}$$

with $\mathbf{0}$ the null matrix,

$$C_4 = \begin{bmatrix} 0 & 0 & -\frac{\omega^4}{12} \\ 0 & 0 & \frac{\omega^4}{12} \\ \frac{\omega^4}{24} & -\frac{\omega^4}{24} & 0 \end{bmatrix}; \tag{13}$$

the matrices A_0 and C_2 are as in Eqs. (8) and (10), and $\sigma_4^2 \equiv (\beta_4^{\mathrm{M}})^2$. The MI gain is now given by the eigenvalue of largest real part of the 12×12 matrix in Eq. (12).

We consider the limit $B_2, B_4 \to 0$. By symbolic manipulation, it is easy to verify that we obtain again Eq. (3) with $\pm\beta_m^{\mathrm{M}}$ in lieu of $\bar{\beta}_m$, for $m = 2, 4$, respectively.

A multi-sidelobe MI gain spectrum is expected as above in Sec. 2.2, because every possible combination of GVD and FOD signs occurs in any realization.

The comparison to numerical results in the next section will show the correctness of this estimates.

3. Numerical results

In order to validate our analytical results, we generate an ensemble of $N_s = 1 \times 10^6$ different GVD (and FOD if applies) profiles and solve equation Eq. (2) exactly for each realization by means of the transfer matrix method [18]. The initial sign of GVD (FOD) is randomized. Telegraph processes are generated according to the method described in Sec. 2. For the sake of definiteness, we take $\gamma P = 1$ and $\beta_2^{\mathrm{M}} = 1$, which is equivalent to defining a nonlinear length $z_{\mathrm{nl}} \equiv (\gamma P)^{-1}$ and a characteristic time $t_0 \equiv \sqrt{\beta_2^{\mathrm{M}} z_{\mathrm{nl}}}$ and to normalizing the propagation distance $z/z_{\mathrm{nl}} \to z$, time $t/t_0 \to t$, field $U/\sqrt{P} \to U$, and FOD $\beta_4^{\mathrm{M}}/((\beta_2^{\mathrm{M}})^2 z_{\mathrm{nl}}) \to \beta_4^{\mathrm{M}}$.

The domain length is set to $L = 20$, initial conditions are chosen to be $(x_1(0), x_2(0))^T = (1, 0)$. For each realization, at the end of the—now deterministic—propagation, we compute $P_{\mathrm{out}} = x_1^2(L) + x_2^2(L)$. The mean gain is defined as

$$\overline{G}_2(\omega; N) \equiv \frac{1}{2L} \ln \left\langle \frac{P_{\mathrm{out}}}{P_{\mathrm{in}}} \right\rangle, \tag{14}$$

where the average is performed on the ensemble and has to be compared to G_2.

3.1. Fluctuations of GVD only, $\bar{\beta}_4 = 0$

As a first example, we consider the effect of an ideal random DM without any FOD contribution, *i.e.*, $\beta_4^{\mathrm{M}} = \bar{\beta}_4 = 0$. In Fig. 2(a) we show a quite short mean length $\bar{L}_2 = 0.2$ (large $B_2 = 10$), comparable to the values studied in [17]. The MI gain consists of one single sidelobe centered around $\omega \approx 2$ and much broader than the conventional MI in anomalous GVD (shown as a dotted black line for comparison), with a maximum about 50% of it. The very large ensemble yields a very smooth $\overline{G}_2$ (solid blue line) that fits almost perfectly to the corresponding G_2 (dashed red line), apart from small ω, due to finite size effects, as explained at length in [17, 21]. If a larger length $\bar{L}_2 = 1.2$ is used, see Fig. 2(b), the MI sidelobe resembles to the conventional MI one, the maximum occurs around $\omega = \sqrt{2}$, but for a smooth tail beyond the convectional cutoff at $\omega = 2$ and a smaller maximum value (about 70% of the convetional one).

To thoroughly assess this properties, we show in Fig. 3 the maximum point $\omega_{\max}$ (a) and its value $G_{\max}$ (b) as a function of $\bar{L}_2$. We notice that both converge for $\bar{L}_2 \to \infty$ to the conventional MI values. The convergence of $\omega_{\max}$ is much faster than that of $G_{\max}$. The discrepancies of this latter at large $\bar{L}_2$ depend on the limited domain length.

3.2. Fluctuations of GVD only, $\bar{\beta}_4 \neq 0$

As a second example, we consider the impact of constant FOD on the ideal random DM, *i.e.*, $\beta_4^{\mathrm{M}} = 0$ but $\bar{\beta}_4 \neq 0$. We take $\bar{L}_2 = 1.2$, as in the example reported in Fig. 2(b).

We show in Fig. 4 the impact of a positive, $\bar{\beta}_4 = 0.25$ in panel (a), or negative, $\bar{\beta}_4 = -0.25$ in panel (b), FOD. As expected, beyond the conventional low-frequency sidelobe, which stems from the anomalous GVD segments, the nonlinear phase-matching condition in Eq. (4) leads to the appearance of an additional MI sidelobe. In Fig. 4(a) this correspond to the position of the high frequency sidelobe predicted by Eq. (3), by substituting $\bar{\beta}_2 \to -\beta_2^{\mathrm{M}}$, *i.e.*, the phase-matching by the segments of anomalous GVD gives rise to a second sidelobe at $\omega \approx 6.77$, which achieves a smaller value of G_2 and is broader than in a homogeneous fiber. Moreover, the primary (baseband) sidelobe attains a larger gain than the secondary one, at variance with the homogeneous counterpart (compare the blue solid to the dotted black line). A similar effect is observed in Fig. 4(b), where by substituting $\bar{\beta}_2 \to \beta_2^{\mathrm{M}}$ in Eq. (3), we can explain the secondary

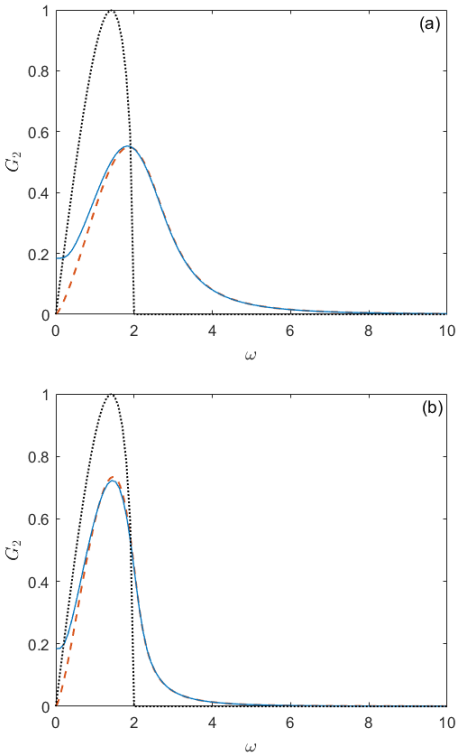

Fig. 2. MI gain as a function of detuning ω for a random GVD distribution with two different average lengths (a) $\bar{L}_2 = 0.2$, (b) $\bar{L}_2 = 1.2$. The numerical results (solid blue curve) are compared to the numerical estimate of Eq. (7) (red dahsed curves) and to the conventional MI gain in a uniform anomalous GVD fiber with $\bar{\beta}_2 = -1$ (black dotted curve).

sidelobe appearing at $\omega \approx 7.06$ (dash-dotted line). The impact of the different FOD sign on the primary MI sidelobe and on the imbalance between the two is negligible.

3.3. *Synchronous fluctuations of GVD and FOD, $\bar{\beta}_4 = 0$*

As a third example, we let both GVD and FOD vary around a null mean value, $\bar{\beta}_2 = \bar{\beta}_4 = 0$, in a synchronous way. We take $\rho = -0.25$ to facilitate the comparison with the previous example in Fig. 4.

We consider two different mean lengths $\bar{L} = \{0.2, 1.2\}$. Therefore, Fig. 5 is compared directly to Fig. 2. For both mean lengths, the primary sidelobe at small ω is indistinguishable if FOD is present or not, like in Fig. 4. A pair of secondary sidelobes appear and turn out to exhibit nearly the same gain of the primary, around 50% and 70% of the conventional one, respectively, as shown above. This is consistent with the discussion in Sec. 2: the sidelobe at $\omega \approx 6.77$ (along with the primary one, see dotted black line) originates from anomalous GVD segments predicted by Eq. (3) by substituting $\bar{\beta}_2 \to -\beta_2^{\mathrm{M}}$, the sidelobe at $\omega \approx 7.06$ (dash-dotted black line) from normal GVD segments, as predicted by Eq. (3) by substituting $\bar{\beta}_2 \to \beta_2^{\mathrm{M}}$. Each segment in the link gives thus rise to an independent phase matching condition and the corresponding MI sidelobe. The choice of $\rho \geq 0$ (not shown) gives obviously only the primary one. As in Fig. 2, the sidelobes are broader for smaller $\bar{L}_2$.

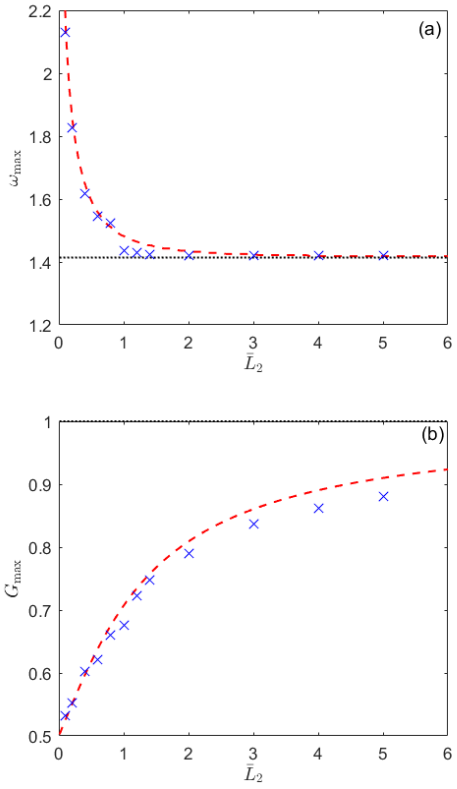

Fig. 3. Comparison of maxima of G_2 and $\overline{G}_2$ as a function $\bar{L}_2$: (a) the maximum points (b) the maximal values. Dashed red lines correpond to the analytical estimates, blue crosses to numerical results. The black dotted line in (a) represents the conventional MI value $\omega = \sqrt{2}$. In panel (b) this limit is $G_2 = 1$.

3.4. Independent fluctuations of GVD and FOD, $\bar{\beta}_4 = 0$

We finally let both GVD and FOD vary independently around a null mean value, $\bar{\beta}_2 = \bar{\beta}_4 = 0$. We take $\beta_4^{\mathrm{M}} = 0.25$ to facilitate the comparison with the previous example in Fig. 5. We assume $\bar{L}_2 = \bar{L}_4 \equiv \bar{L}$. We consider again two different mean lengths $\bar{L} = \{0.2, 1.2\}$. Therefore, Fig. 6 is compared directly to Fig. 5. The primary sidelobe at small ω is again indistinguishable if FOD is present or not, apart from the tails connecting it to the secondary sidelobes (in the $3 < \omega < 5$ range). These latter, stemming from the fluctuations of FOD, exhibit instead several peculiar properties, quite different from those found for synchronous fluctuations. For $\bar{L} = 0.2$, a small sidelobe occurs at $\omega \approx 6.92$ and is about 6 times smaller than the first one. For larger $\bar{L} = 1.2$ the secondary sidelobe splits into two—we verify that they start to be distinughible at $\bar{L} = 0.8$ (not shown). By comparing to the MI gain given by every possible homogeneous limit, *i.e.*, every combination of $(\bar{\beta}_2 \to \pm\beta_2^{\mathrm{M}}, \bar{\beta}_4 \to \pm\beta_4^{\mathrm{M}})$—dotted (dash-dotted) black lines for $\bar{\beta}_2 < 0$ ($\bar{\beta}_2 > 0$), respectively—it is apparent that the pair of secondary sidelobes correspond to the same nonlinear phase-matching conditions discussed above in reference to Fig. 4(a) and 4(b), respectively, and to Fig. 5. The independent oscillations of GVD and FOD give rise, effectively, to all the possible phase-matching conditions being satisfied and thus to three independent maxima of G_2. The secondary lobes achieve a smaller G_2 in Fig. 6(b) (54% of the value of the primary one) than in Figs. 4 and 5(b), on account of the FOD stochasticity. As discussed in [17], larger ω are more

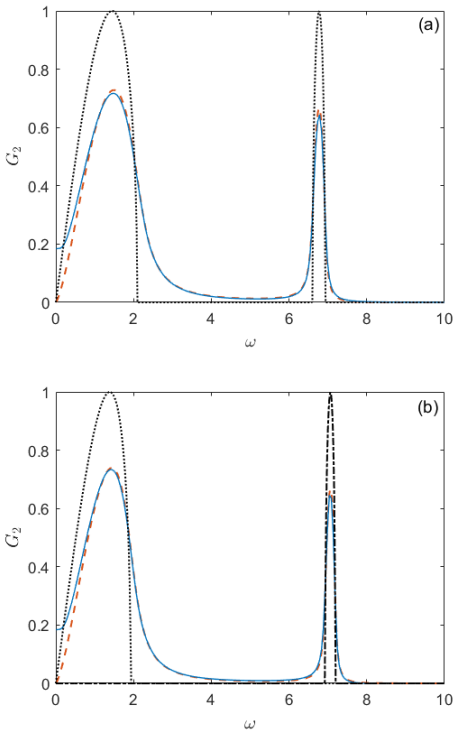

Fig. 4. MI gain as a function of detuning ω for a random GVD distribution with intermediate $\bar{L}_2 = 1.2$ and fixed FOD. As in Fig. 2, the numerical results (solid blue curve) are compared to the numerical estimate of Eq. (7) (red dahsed curves). The dotted lines show the MI gain in a uniform anomalous GVD fiber with $\bar{\beta}_2 = -1$ and positive (negative) FOD in (a) [resp. (b)], while the additional dash-dotted line in panel (b) shows the MI gain in a uniform normal GVD fiber with $\bar{\beta}_2 = 1$ and negative FOD. Chosen values of FOD are (a) $\overline{\beta}_4 = 0.25$, (b) $\overline{\beta}_4 = -0.25$.

sensitive to lowpass random fluctuations, because the associated wavelength is smaller and thus comparable to the mean length. Combining random fluctuations on two parameters amplifies this effect.

4. Conclusions

We studied a specific (lowpass) colored stochastic process, the telegraph process, as a fluctuation of group-velocity dispersion around a zero mean value. This resembles a random dispersion-manged fiber link. We show how the modulational instability sidebands behave as a function of the mean *waiting* length between sign changes: for a short mean length the MI sidelobes are broader and smaller than their conventional counterpart, but they converge to them for a long mean length (several times the nonlinear length). We included also, as an additional refinement, the effect of a constant or variable FOD. A constant FOD (pertinent if the operation point is close to zero-dispersion point) yields an additional sideband, centered around an easily predictable detuning. Fluctuating FOD may give rise to a pair of closely separated secondary lobes, which correspond to the set of all the sidelobes in normal or anomalous GVD, with different FOD signs. Similarly to the MI gain in a homogenous fiber, where even-order ($2n$) high-order dispersion yields a family of up to n sidelobes of equal maximum gain, the stochastic counterpart shows

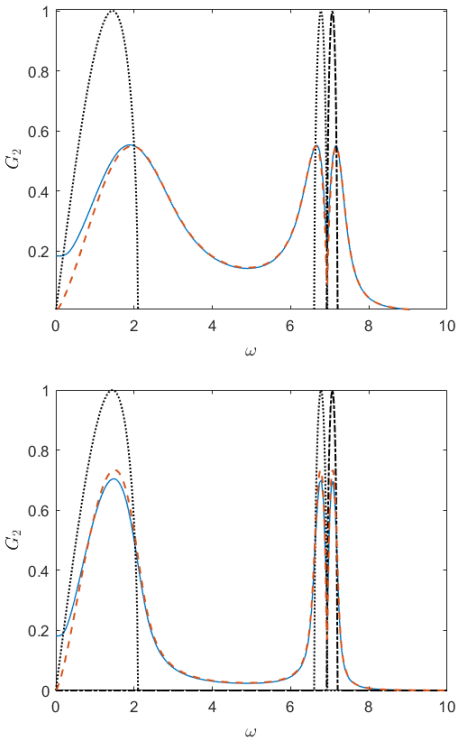

Fig. 5. Same as in Fig. 4 for random and synchronous GVD and FOD with (a) $\bar{L} = 0.2$, (b) $\bar{L} = 1.2$. The dotted lines correspond here to the gain in a homogeneous fiber with $\bar{\beta}_2 = -1$, $\bar{\beta}_4 = 0.25$, the dash-dotted lines to $\bar{\beta}_2 = 1$, $\bar{\beta}_4 = -0.25$. The MI sidelobe $\bar{\beta}_2 = -1$, $\bar{\beta}_4 = -0.25$ is almost identical to the conventional MI shown in Fig. 2 and is omitted.

balanced sidelobes for synchronous fluctuations. This is not the case for GVD variations around constant FOD or independent GVD and FOD variations, where the baseband is larger than the high-frequency sidelobes. For short correlation lengths, a single merged high-frequency sidelobe appears for independent GVD and FOD variations. In every example, the analytical estimates obtained by the analytical approach we employ here (after M. Gitterman's work) match almost perfectly with the numerical data.

A few other combinations of GVD and FOD could be analyzed, but for the sake of brevity we decided to focus on just four of them, which we find of more practical interest. A pure FOD fluctuation will yield a negligible MI gain, as in Ref. [17] for pure GVD, if $\bar{\beta}_4 \neq 0$ or else converge to the FOD gain profile [6], *i.e.*, a quadratic growth for small ω. Fluctuations of GVD around $\bar{\beta}_2 = 0$, associated to $\bar{\beta}_4 \neq 0$ and $\beta_4^{\mathrm{M}} \neq 0$ yield a proliferation of MI sidebands, satisfying all the admissible nonlinear phase-matching conditions as explained in the present work.

We limited ourselves to the linearized NLSE, which models the initial growth of unstable sidebands. The nonlinear stage which takes place as soon as enough energy is converted from the pump P to sidebands is not considered here. Several studies are devoted to nonlinear oscillators with multiplicative noise, see for example [32, 33]. Their application to optical fibers will be the object of a future study.

Our results may permit to tailor MI gain sidebands in optical fibers by means of stochastic GVD fluctuations and suggest the regimes to achieve that. For example, such discrete fluctuations

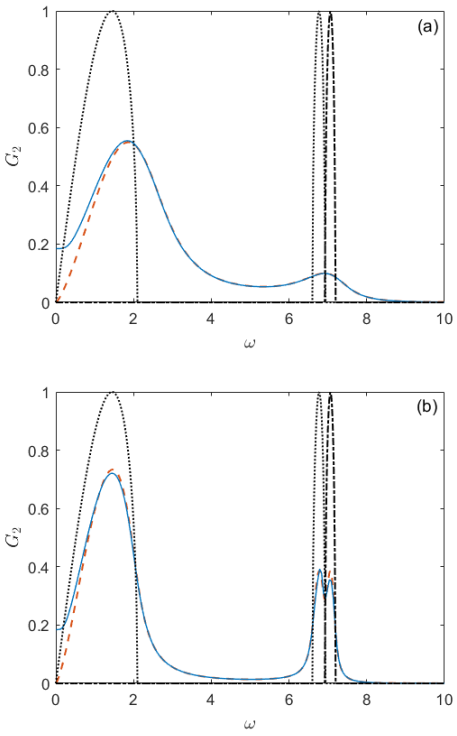

Fig. 6. Same as in Fig. 5 for random and independent GVD and FOD with (a) $\bar{L} = 0.2$, (b) $\bar{L} = 1.2$.

can be implemented by means of fiber splicing.

Funding. The present research was supported by IRCICA (USR 3380 CNRS), Agence Nationale de la Recherche (Programme Investissements d'Avenir, I-SITE VERIFICO, Labex CEMPI); Ministry of Higher Education and Research; Hauts de France Council; European Regional Development Fund (Photonics for Society P4S, Wavetech); Italian Ministry of Higher Education and Research, PRIN grants (2020X4T57A, 20222NCTCY)

Acknowledgments. We thank S. De Bièvre and G. Dujardin of Laboratoire Paul Painlevé for fruitful discussions.

Disclosures. The authors declare no conflicts of interest.

Data availability. Data underlying the results presented in this paper are not publicly available at this time but may be obtained from the authors upon reasonable request.

References

1. V. E. Zakharov and L. A. Ostrovsky, "Modulation instability: The beginning," Phys. D: Nonlinear Phenom. **238**, 540–548 (2009).
2. V. I. Bespalov and V. I. Talanov, "Filamentary structure of light beams in nonlinear liquids," ZhETF Pis ma Redaktsiiu **3**, 471 (1966).
3. T. B. Benjamin and J. E. Feir, "The disintegration of wave trains on deep water Part 1. Theory," J. Fluid Mech. **27**, 417 (1967).
4. V. E. Zakharov, "Stability of periodic waves of finite amplitude on the surface of a deep fluid," J. Appl. Mech. Tech. Phys. **9**, 190–194 (1968).
5. K. Tai, A. Hasegawa, and A. Tomita, "Observation of modulational instability in optical fibers," Phys. Rev. Lett. **56**, 135–138 (1986).

6. S. B. Cavalcanti, J. C. J. C. Cressoni, H. R. da Cruz, and A. S. Gouveia-Neto, "Modulation instability in the region of minimum group-velocity dispersion of single-mode optical fibers via an extended nonlinear Schrödinger equation," Phys. Rev. A **43**, 6162–6165 (1991).
7. F. Biancalana and D. V. Skryabin, "Vector modulational instabilities in ultra-small core optical fibres," J. Opt. A: Pure Appl. Opt. **6**, 301–306 (2004).
8. N. J. Smith and N. Doran, "Modulational instabilities in fibers with periodic dispersion management." Opt. letters **21**, 570–2 (1996).
9. F. K. Abdullaev, S. A. Darmanyan, A. Kobyakov, and F. Lederer, "Modulational instability in optical fibers with variable dispersion," Phys. Lett. A **220**, 213–218 (1996).
10. M. Droques, A. Kudlinski, G. Bouwmans, G. Martinelli, and A. Mussot, "Experimental demonstration of modulation instability in an optical fiber with a periodic dispersion landscape." Opt. letters **37**, 4832–4 (2012).
11. A. Armaroli and F. Biancalana, "Tunable modulational instability sidebands via parametric resonance in periodically tapered optical fibers," Opt. Express **20**, 25096 (2012).
12. A. Mussot, M. Conforti, S. Trillo, F. Copie, and A. Kudlinski, "Modulation instability in dispersion oscillating fibers," Adv. Opt. Photonics **10**, 1 (2018).
13. F. K. Abdullaev and J. Garnier, "Modulational instability of electromagnetic waves in birefringent fibers with periodic and random dispersion," Phys. Rev. E **60**, 1042–1050 (1999).
14. J. Garnier and F. K. Abdullaev, "Modulational instability induced by randomly varying coefficients for the nonlinear Schrödinger equation," Phys. D: Nonlinear Phenom. **145**, 65–83 (2000).
15. M. Chertkov, I. Gabitov, and J. Moeser, "Pulse confinement in optical fibers with random dispersion," Proc. National Acad. Sci. United States Am. **98**, 14208–14211 (2001).
16. G. Dujardin, A. Armaroli, S. R. Nodari, A. Mussot, A. Kudlinski, S. Trillo, M. Conforti, S. De Bièvre, and S. De Bievre, "Modulational instability in optical fibers with randomly kicked normal dispersion," Phys. Rev. A **103**, 053521 (2021).
17. A. Armaroli, G. Dujardin, A. Kudlinski, A. Mussot, S. Trillo, S. De Bièvre, and M. Conforti, "Stochastic modulational instability in the nonlinear Schrödinger equation with colored random dispersion," Phys. Rev. A **105**, 013511 (2022).
18. G. P. Agrawal, *Nonlinear Fiber Optics* (Academic Press, Oxford, 2012), fifth edit ed.
19. S. K. Turitsyn, B. G. Bale, and M. P. Fedoruk, "Dispersion-managed solitons in fibre systems and lasers," Phys. Reports **521**, 135–203 (2012).
20. B. A. Malomed and A. Berntson, "Propagation of an optical pulse in a fiber link with random-dispersion management," J. Opt. Soc. Am. B **18**, 1243 (2001).
21. A. Armaroli, G. Dujardin, A. Kudlinski, A. Mussot, S. De Bièvre, and M. Conforti, "Modulational instability in randomly dispersion-managed optical fiber links," Phys. Rev. A **108**, 023510 (2023).
22. K. Furutsu, "On the statistical theory of electromagnetic waves in a fluctuating medium (I)," J. Res. National Bureau Stand. Sect. D: Rádió Propag. **67D**, 303 (1963).
23. E. A. Novikov, "Functionals and the Random-force Method in Turbulence Theory," JETP **20**, 1290–1294 (1965).
24. V. E. Shapiro and V. M. Loginov, ""Formulae of differentiation" and their use for solving stochastic equations," Phys. A: Stat. Mech. its Appl. **91**, 563–574 (1978).
25. M. Gitterman, *Noisy Oscillator, The: Random Mass, Frequency, Damping* (World Scientific Publishing Co. Pte. Ltd., 2005).
26. M. Gitterman, "Classical harmonic oscillator with multiplicative noise," Phys. A: Stat. Mech. its Appl. **352**, 309–334 (2005).
27. V. I. Klyatskin, *Lectures on Dynamics of Stochastic Systems* (Elsevier, Amsterdam, 2010), 1st ed.
28. H. M. Taylor and S. Karlin, *An Introduction To Stochastic Modeling* (Academic Press, 1998), third edition ed.
29. S. Pitois and G. Millot, "Experimental observation of a new modulational instability spectral window induced by fourth-order dispersion in a normally dispersive single-mode optical fiber," Opt. Commun. **226**, 415–422 (2003).
30. N. Van Kampen, *Stochastic Processes in Physics and Chemistry* (Elsevier, 2007).
31. S. Burov and M. Gitterman, "Noisy oscillator: Random mass and random damping," Phys. Rev. E **94**, 052144 (2016).
32. K. Mallick and P. Marcq, "Anomalous diffusion in nonlinear oscillators with multiplicative noise," Phys. Rev. E - Stat. Physics, Plasmas, Fluids, Relat. Interdiscip. Top. **66**, 14 (2002).
33. K. Mallick and P. Marcq, "Effects of parametric noise on a nonlinear oscillator," Phys. A: Stat. Mech. its Appl. **325**, 213–219 (2003).